

High-Throughput FPGA-based QC-LDPC Decoder Architecture

Swapnil Mhaske*, Hojin Kee†, Tai Ly†, Ahsan Aziz†, Predrag Spasojevic*

*Wireless Information Network Laboratory, Rutgers University, New Brunswick, NJ, USA

Email: {swapnil.mhaske@rutgers.edu, spasojev@winlab.rutgers.edu}

†National Instruments Corporation, Austin, TX, USA

Email: {hojin.kee, tai.ly, ahsan.aziz}@ni.com

Abstract—We present an efficient and scalable high-throughput FPGA-based architecture for the Min-Sum Algorithm (MSA) based decoder for Quasi-Cyclic Low-Density Parity-Check (QC-LDPC) codes. We present a compact representation of the parity-check matrix (PCM) which allows for a significant improvement in throughput (3x in our case study) compared to conventional methods. In spite of the compact representation, layer-pipelined processing is performed with minimum overhead by partitioning the parity-check matrix into superlayers and by staggered processing of blocks within each superlayer. As a case study, a MSA based decoder for the rate-1/2, 1944-bit, irregular QC-LDPC code specified in the *IEEE 802.11n (2012)* standard [1] is implemented on the *Xilinx Kintex-7* FPGA with the help of the *FPGA IP* compiler available in the *National Instruments LabVIEW Communication System Design Suite (CSDS)*. This compiler offers an automated and systematic compilation flow which generates an optimized hardware implementation from the LDPC algorithm in approximately 3 minutes. The decoder achieves an overall throughput of 608Mb/s at an operating frequency of 200MHz. As per our knowledge this is the fastest implementation of an *IEEE 802.11n* compliant QC-LDPC decoder using an algorithmic compiler.

Index Terms—5G, mm-wave, QC-LDPC, Belief Propagation (BP) decoding, MSA, layered decoding, high-level synthesis (HLS), FPGA, IEEE 802.11n.

I. INTRODUCTION

By the year 2020, wireless data traffic is expected to increase by a 1000 fold [2]. More than 50 billion devices with a wide range of application requirements will be connected to these wireless networks, making it a highly heterogeneous network. Peak data rates are slated to be upto ten gigabits per second (Gb/s) with an overall latency of less than 1ms [3]. The next generation of wireless technology being envisioned and researched today is collectively termed as Beyond-4G and 5G wireless (hereafter referred to as 5G). The dominant thrust of 5G research is the migration to higher frequencies to exploit the larger bandwidths available in the 30-300GHz range. However, operation in this spectrum comes with challenges such as, reliance on line of sight (LOS) communication, short range of communication, significantly increased shadowing loss and rapid fading in time. Although techniques such as large antenna arrays and rapidly adaptive beamsteering can overcome propagation loss and dynamic fading, they will significantly increase the overall processing complexity of the system, especially at the area and power constrained mobile terminal.

A well designed channel coding system can be a major contributor to the performance gain in a communication system. With the significant increase in processing at the physical layer (relative to current generation systems such as 4G LTE), the processing budget in terms of time, area and power available to the channel encoder and decoder will further decrease. Thus, there is a need to develop coding structures that allow for multi-Gb/s implementations with latency of the order of a microsecond and with a smaller silicon footprint.

To adapt to the evolving requirements and specifications for 5G technology, hardware solutions must be reconfigurable and scalable, yet delivering state-of-the-art performance. Given the processing and rapid-prototyping capabilities of contemporary FPGAs, (compared to an ASIC solution) we focus on an FPGA-based solution for our channel coding research.

The main contribution of this brief is the compact representation of the parity-check matrix (PCM) which, in general for a QC-LDPC code (based on circulant-1 identity matrix construction as explained in Section II), provides multiple-fold increase (3-fold in the case study) in the throughput performance of the decoder. With this alternate representation, we provide without loss of generality, a method to process compacted blocks in two layers in a pipelined manner as shown in Section III-E. The FPGA IP compiler translates graphical algorithmic dataflow description to a hardware description language (VHDL) which generates an optimized hardware implementation from the LDPC algorithm in approximately 3 minutes. For the initial phase of this project, the strategies that we have proposed are validated by a successful running implementation of a standard compliant QC-LDPC decoder. An application of this decoder implementation that achieves over 2Gb/s throughput is also demonstrated.

The remainder of this paper is organized as follows. Section II describes the QC-LDPC codes and the decoding algorithm chosen for this implementation. The strategies for achieving high throughput are explained in Section III. The case study for *IEEE 802.11n (2012)* is described in Section IV, and finally we conclude with Section V.

II. QUASI-CYCLIC LDPC CODES AND DECODING

LDPC codes (due to R. Gallager [4]) are a class of linear block codes that have been shown to achieve near-capacity

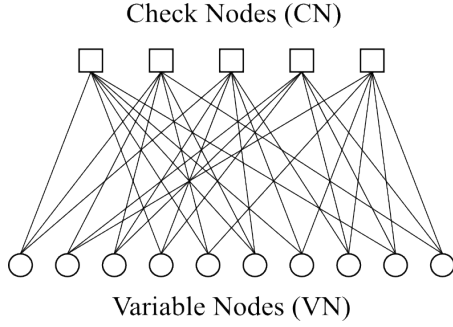


Figure 1: A Tanner graph where VNs (representing the code bits) are shown as circles and CNs (representing the parity-check equations) are shown as squares. Each edge in the graph corresponds to a non-zero entry (1 for binary LDPC codes) in the PCM \mathbf{H} .

performance on a broad range of channels and are characterized by a low-density (sparse) PCM representation.

Mathematically, an LDPC code is a null-space of its $m \times n$ PCM \mathbf{H} , where m denotes the number of parity-check equations or parity-bits and n denotes the number of variable nodes or code bits [5]. In other words, for a rank m PCM \mathbf{H} , m is the number of redundant bits added to the k information bits, which together form the codeword of length $n = k + m$. In the Tanner graph representation (due to Tanner [6]), \mathbf{H} is the incidence matrix of a bipartite graph comprising of two sets: the check node (CN) set of m parity-check equations and the variable node (VN) set of n variable or bit nodes; the i^{th} CN is connected to the j^{th} VN if $\mathbf{H}(i, j) = 1$, $1 \leq i \leq m$ and $1 \leq j \leq n$. A toy example of a Tanner graph is shown in Fig. 1. The degree d_{c_i} (d_{v_j}) of a CN i (VN j) is equal to the number of 1s along the i^{th} row (j^{th} column) of \mathbf{H} . For constants $c_c, c_v \in \mathbb{Z}_{>0}$ and $c_c \ll m, c_v \ll n$, if $\forall i, j$, $d_{c_i} = c_c$ and $d_{v_j} = c_v$, then the LDPC code is called as a regular code and is called an irregular code otherwise.

A. Quasi-Cyclic LDPC Codes

The first LDPC codes by Gallager are random, which complicate the decoder implementation, mainly because a random interconnect pattern between the VNs and CNs directly translates to a complex wire routing circuit on hardware. QC-LDPC codes belong to the class of structured codes that are relatively easier to implement without significantly compromising performance.

The construction of identity matrix based QC-LDPC codes relies on an $m_b \times n_b$ matrix \mathbf{H}_b sometimes called as the *base matrix* which comprises of cyclically right-shifted identity and zero submatrices both of size $z \times z$ where, $z \in \mathbb{Z}^+$, $1 \leq i_b \leq (m_b)$ and $1 \leq j_b \leq (n_b)$, the shift value,

$$s = \mathbf{H}_b(i_b, j_b) \in \mathcal{S} = \{-1\} \cup \{0, \dots, z-1\}$$

The PCM matrix \mathbf{H} is obtained by *expanding* \mathbf{H}_b using the mapping,

$$s \longrightarrow \begin{cases} \mathbf{I}_s, & s \in \mathcal{S} \setminus \{-1\} \\ \mathbf{0}, & s \in \{-1\} \end{cases}$$

where, \mathbf{I}_s is an identity matrix of size z which is cyclically right-shifted by $s = \mathbf{H}_b(i_b, j_b)$ and $\mathbf{0}$ is the all-zero matrix of size $z \times z$. As \mathbf{H} is composed of the submatrices \mathbf{I}_s and $\mathbf{0}$, it has $m = m_b \cdot z$ rows and $n = n_b \cdot z$ columns. \mathbf{H} for the *IEEE 802.11n (2012)* standard [1] (used for our case study) with $z = 81$ is shown in Table I.

B. Scaled Min-Sum Algorithm for Decoding QC-LDPC Codes

LDPC codes can be decoded using message passing (MP) or belief propagation (BP) [4], [7] on the bipartite Tanner graph where, the CNs and VNs communicate with each other, successively passing revised estimates of the log-likelihood ratio (LLR) associated, in every decoding iteration. In this work we have employed the efficient decoding algorithm presented in [8], with pipelined processing of layers based on the row-layered decoding technique [9], detailed in Section III-C.

Definition 1. For $1 \leq i \leq m$ and $1 \leq j \leq n$, let v_j denote the j^{th} bit in the length n codeword and $y_j = v_j + n_j$ denote the corresponding received value from the channel corrupted by the noise sample n_j . Let the variable-to-check (VTC) message from VN j to CN i be q_{ij} and, let the check-to-variable (CTV) message from CN i to VN j be r_{ij} . Let the a posteriori probability (APP) ratio for VN j be denoted as p_j .

The steps of the scaled-MSA [5], [10] are given below.

- 1) Initialize the APP ratio and the CTV messages as,

$$p_j^{(0)} = \ln \left\{ \frac{P(v_j = 0 | y_j)}{P(v_j = 1 | y_j)} \right\}, \quad 1 \leq j \leq n \quad (1)$$

$$r_{ij}^{(0)} = 0, \quad 1 \leq i \leq m, 1 \leq j \leq n$$

- 2) Iteratively compute at the t^{th} decoding iteration,

$$q_{ij}^{(t)} = p_j^{(t-1)} - r_{ij}^{(t-1)} \quad (2)$$

$$r_{ij}^{(t)} = a \cdot \prod_{k \in \mathcal{N}(i) \setminus \{j\}} \text{sign}(q_{ik}^{(t)}) \cdot \min_{k \in \mathcal{N}(i) \setminus \{j\}} \{|q_{ik}^{(t)}|\} \quad (3)$$

$$p_j^{(t)} = q_{ij}^{(t)} + r_{ij}^{(t)} \quad (4)$$

where, $1 \leq i \leq m$, and $k \in \mathcal{N}(i) \setminus \{j\}$ represents the set of the VN neighbors of CN i excluding VN j . Let t_{max} be the maximum number of decoding iterations.

- 3) Decision on the code bit v_j , $1 \leq j \leq n$ as,

$$\hat{v}_j = \begin{cases} 0, & p_j < 0 \\ 1, & \text{otherwise} \end{cases} \quad (5)$$

- 4) If $\hat{\mathbf{v}}\mathbf{H}^T = \mathbf{0}$, where $\hat{\mathbf{v}} = (\hat{v}_1, \hat{v}_2, \dots, \hat{v}_n)$, or $t = t_{max}$, declare $\hat{\mathbf{v}}$ as the decoded codeword.

It is well known that since the MSA is an approximation of the SPA, the performance of the MSA is relatively worse than the SPA [5]. However, in [10] it has been shown that scaling the CTV messages r_{ij} can improve the performance of the MSA. Hence, we scale the CTV messages by a factor a ($=0.75$).

Layers ↓	Blocks →																								
	B ₁	B ₂	B ₃	B ₄	B ₅	B ₆	B ₇	B ₈	B ₉	B ₁₀	B ₁₁	B ₁₂	B ₁₃	B ₁₄	B ₁₅	B ₁₆	B ₁₇	B ₁₈	B ₁₉	B ₂₀	B ₂₁	B ₂₂	B ₂₃	B ₂₄	
L ₁	57	-1	-1	-1	50	-1	11	-1	50	-1	79	-1	1	0	-1	-1	-1	-1	-1	-1	-1	-1	-1	-1	-1
L ₂	3	-1	28	-1	0	-1	-1	-1	55	7	-1	-1	-1	0	0	-1	-1	-1	-1	-1	-1	-1	-1	-1	-1
L ₃	30	-1	-1	-1	24	37	-1	-1	56	14	-1	-1	-1	-1	0	0	-1	-1	-1	-1	-1	-1	-1	-1	-1
L ₄	62	53	-1	-1	53	-1	-1	3	35	-1	-1	-1	-1	-1	-1	0	0	-1	-1	-1	-1	-1	-1	-1	-1
L ₅	40	-1	-1	20	66	-1	-1	22	28	-1	-1	-1	-1	-1	-1	-1	0	0	-1	-1	-1	-1	-1	-1	-1
L ₆	0	-1	-1	-1	8	-1	42	-1	50	-1	-1	8	-1	-1	-1	-1	-1	0	0	-1	-1	-1	-1	-1	-1
L ₇	69	79	79	-1	-1	-1	56	-1	52	-1	-1	-1	0	-1	-1	-1	-1	-1	0	0	-1	-1	-1	-1	-1
L ₈	65	-1	-1	-1	38	57	-1	-1	72	-1	27	-1	-1	-1	-1	-1	-1	-1	-1	0	0	-1	-1	-1	-1
L ₉	64	-1	-1	-1	14	52	-1	-1	30	-1	-1	32	-1	-1	-1	-1	-1	-1	-1	-1	0	0	-1	-1	-1
L ₁₀	-1	45	-1	70	0	-1	-1	-1	77	9	-1	-1	-1	-1	-1	-1	-1	-1	-1	-1	-1	0	0	-1	-1
L ₁₁	2	56	-1	57	35	-1	-1	-1	-1	-1	12	-1	-1	-1	-1	-1	-1	-1	-1	-1	-1	-1	0	0	-1
L ₁₂	24	-1	61	-1	60	-1	-1	27	51	-1	-1	16	1	-1	-1	-1	-1	-1	-1	-1	-1	-1	-1	-1	0

Table I: Base matrix \mathbf{H}_b for $z = 81$ specified in IEEE 802.11n (2012) standard used in the case study. $L_1 - L_{12}$ are the layers and $B_1 - B_{24}$ are the block columns (see Section III-C). Valid blocks (see section III-D) are highlighted.

Remark 1. The standard MP algorithm is based on the so-called *flooding* or *two-phase* schedule where, each decoding iteration comprises of two phases. In the first phase, VTC messages for all the VNs are computed and, in the second phase the CTV messages for all the CNs are computed, strictly in that order. Thus, message updates from one side of the graph propagate to the other side only in the next decoding iteration. In the algorithm given in [8] however, message updates can propagate across the graph in the same decoding iteration. This provides advantages [8] such as, a single processing unit is required for both CN and VN message updates, memory storage is reduced on account of the on-the-fly computation of the VTC messages q_{ij} and the algorithm converges faster than the standard MP flooding schedule requiring fewer decoding iterations.

III. TECHNIQUES FOR HIGH-THROUGHPUT

To understand the high-throughput requirements for LDPC decoding, let us first define the decoding throughput T of an iterative LDPC decoder.

Definition 2. Let F_c be the clock frequency, n be the code length, N_i be the number of decoding iterations and N_c be the number of clock cycles per decoding iteration, then the throughput of the decoder is given by, $T = \frac{F_c \cdot n}{N_i \cdot N_c}$ b/s

Even though, n and N_i are functions of the code and the decoding algorithm used, F_c and N_c are determined by the hardware architecture. Architectural optimization such as the ability to operate the decoder at higher clock rates with minimal latency between decoding iterations can help

achieve higher throughput. We have employed the following techniques to increase the throughput given by Definition 2.

A. Linear Complexity Node Processing

As noted in Section II-B, separate processing units for CNs and VNs are not required unlike that for the flooding schedule. The hardware elements that process equations (2)-(4) are collectively referred to as the Node Processing Unit (NPU).

Careful observation reveals that, among equations (2)-(4), processing the CTV messages r_{ij} , $1 \leq i \leq m$ and $1 \leq j \leq n$ is the most computationally intensive due to the calculation of the sign, and the minimum value operations. The complexity of processing the minimum value is $\mathcal{O}(d_{c_i}^2)$. In software, this translates to two nested for-loops, an outer loop that executes d_{c_i} times and an inner loop that executes $(d_{c_i} - 1)$ times.

To achieve linear complexity $\mathcal{O}(d_{c_i})$ for the minimum value computation, we split the process into two phases or passes: the *global* pass where the first and the second minimum (the smallest value in the set excluding the minimum value of the set) for all the neighboring VNs of a CN are computed and the *local* pass where the first and second minimum from the global pass are used to compute the minimum value for each neighboring VN. Based on the functionality of the two passes, the NPU is divided into the Global NPU (GNPU) and the Local NPU (LNPU). The algorithm is given below.

1) Global Pass:

- i. *Initialization:* Let ℓ denote the discrete time-steps such that, $\ell \in \{0\} \cup \{1, 2, \dots, |\mathcal{N}(i)|\}$ and let $f^{(\ell)}$ and $s^{(\ell)}$ denote the value of the first and the second minimum

at time ℓ respectively. The initial value at time $\ell = 0$ is,

$$f^{(0)} = s^{(0)} = \infty. \quad (6)$$

ii. *Comparison*: Let $k_i(\ell) \in \mathcal{N}(i)$, $\ell = \{1, 2, \dots, |\mathcal{N}(i)|\}$, denote the index of the ℓ^{th} neighboring VN of CN i . Note that, $k_i(\ell)$ depends on i and ℓ , specifically, for a given CN i it is a bijective function of ℓ . An increment from $(\ell - 1)$ to ℓ corresponds to moving from the edge CN $i \leftrightarrow$ VN $k_i(\ell - 1)$ to the edge CN $i \leftrightarrow$ VN $k_i(\ell)$.

$$f^{(\ell)} = \begin{cases} |q_{ik_i(\ell)}|, & |q_{ik_i(\ell)}| \leq f^{(\ell-1)} \\ f^{(\ell-1)}, & \text{otherwise.} \end{cases} \quad (7)$$

$$s^{(\ell)} = \begin{cases} |q_{ik_i(\ell)}|, & f^{(\ell-1)} < |q_{ik_i(\ell)}| < s^{(\ell-1)} \\ f^{(\ell-1)}, & |q_{ik_i(\ell)}| \leq f^{(\ell-1)} \\ s^{(\ell-1)}, & \text{otherwise.} \end{cases} \quad (8)$$

Thus, $f^{(\ell_{max})}$ and $s^{(\ell_{max})}$ are the first and second minimum values for the set of VN neighbors of CN i , where, $\ell_{max} = |\mathcal{N}(i)|$.

2) *Local Pass*: Let the minimum value as per equation (3) for VN $k_i(\ell)$ be denoted as $q_{ik_i(\ell)}^{min}$, $\ell \in \{1, 2, \dots, |\mathcal{N}(i)|\}$ then,

$$q_{ik_i(\ell)}^{min} = \begin{cases} f^{(\ell_{max})}, & |q_{ik_i(\ell)}| \neq f^{(\ell_{max})} \\ s^{(\ell_{max})}, & \text{otherwise.} \end{cases} \quad (9)$$

In software, this translates to two consecutive for-loops, each executing $(d_{c_i} - 1)$ times. Consequently, this reduces the complexity from $\mathcal{O}(d_{c_i}^2)$ to $\mathcal{O}(d_{c_i})$. A similar approach is also found in [11], [12]. The sign computation is processed in a similar manner.

B. z -fold Parallelization of NPUs

The CN message computation given by equation (3) is repeated m times in a decoding iteration i.e. once for each CN. A straightforward serial implementation of this kind is slow and undesirable. Instead, we apply a strategy based on the following understanding.

Fact 1. *An arbitrary submatrix \mathbf{I}_s in the PCM \mathbf{H} corresponds to z CNs connected to z VNs on the bipartite graph, with strictly 1 edge between each CN and VN.*

This implies that no CN in this set of z CNs given by \mathbf{I}_s shares a VN with another CN in the same set. This presents us with an opportunity to operate z NPUs in parallel (hereafter referred to as an *NPU array*), resulting in a z -fold increase in throughput.

C. Layered Decoding

From Remark 1 it is clear that, in the flooding schedule *all* nodes on one side of the bipartite graph can be processed in parallel. Although, such a *fully parallel* implementation may seem as an attractive option for achieving high-throughput performance, it has its own drawbacks. Firstly, it becomes

quickly intractable in hardware due to the complex interconnect pattern. Secondly, such an implementation usually restricts itself to a specific code structure. In spite of the serial nature of the algorithm in II-B, one can process multiple nodes at the same time if the following condition is satisfied.

Fact 2. *From the perspective of CN processing, two or more CNs can be processed at the same time (i.e. they are independent of each other) if they do not have one or more VNs (code bits) in common.*

The row-layering technique used in this work essentially relies on the above condition being satisfied. In terms of \mathbf{H} , an arbitrary subset of rows can be processed at the same time provided that, no two or more rows have a 1 in the same column of \mathbf{H} . This subset of rows is termed as a *row-layer* (hereafter referred to as a *layer*). In other words, given a set $\mathcal{L} = \{L_1, L_2, \dots, L_I\}$ of I layers in \mathbf{H} , $\forall u \in \{1, 2, \dots, I\}$ and $\forall i, i' \in L_u$, then, $\mathcal{N}(i) \cap \mathcal{N}(i') = \phi$.

Observing that, $\sum_{u=1}^I |L_u| = m$, in general, L_u can be any subset of rows as long as the rows within each subset satisfy the condition in Fact 2; implying that, $|L_u| \neq |L_{u'}|$, $\forall u, u' \in \{1, 2, \dots, I\}$ is possible. Owing to the structure of QC-LDPC codes, the choice of $|L_u|$ (and hence I) becomes much obvious. Submatrices \mathbf{I}_s in \mathbf{H}_b (with row and column weight of 1) guarantee that, for the z CNs corresponding to the rows of \mathbf{I}_s , always satisfy the condition in Fact 2. Hence, $|L_u| = |L_{u'}| = z$ is chosen.

From the VN or column perspective, $|L_u| = z$, $\forall u = \{1, 2, \dots, I\}$ implies that, the columns of \mathbf{H} are also divided into subsets of size z (hereafter referred to as *block columns*) given by the set $\mathcal{B} = \{B_1, B_2, \dots, B_J\}$, $J = \frac{n}{z} = n_b$. Observing that VNs belonging to a block column may participate in CN equations across several layers, we further divide the block columns into *blocks*, where a block is the intersection of a layer and a block column. Two or more layers $L_u, L_{u'}$ are said to be *dependent* with respect to the block column B_w if, $\mathbf{H}_b(u, w) \neq -1$ and, $\mathbf{H}_b(u', w) \neq -1$ and are said to be *independent* otherwise. For example, in Table I we can see that layers L_4, L_7, L_{10} and L_{11} are dependent with respect to block column B_2 . Thus, layer L_7 cannot begin updating the VNs associated with block column B_2 before layer L_4 has finished updating messages for the same set of VNs and so on. The idea of parallelizing z NPUs seen in Section III-B can be extended to layers, NPU arrays can process message updates for multiple independent layers. In Section III-E, we discuss pipelining methods that allow us to overcome layer-to-layer dependency and improve throughput.

D. Compact Representation of \mathbf{H}_b

Before we discuss the pipelined processing of layers, we present a novel compact (thus efficient) matrix representation leading to a significant improvement in throughput. To understand this, let us call $\mathbf{0}$ submatrices in \mathbf{H} as *invalid* blocks, where there are no edges between the corresponding CNs and VNs, and the submatrices \mathbf{I}_s as *valid* blocks. In a conventional approach to scheduling (for example in [13]),

message computation is done for all the valid and invalid blocks. To avoid processing invalid blocks, we propose an alternate representation of \mathbf{H}_b in the form of two matrices: β_I , the block index matrix and β_S , the block shift matrix. β_I

Layers ↓	Blocks →							
	b ₁	b ₂	b ₃	b ₄	b ₅	b ₆	b ₇	b ₈
L ₁	0	4	6	8	10	12	13	-1
L ₂	0	2	4	8	9	13	14	-1
L ₃	0	4	5	8	9	14	15	-1
L ₄	0	1	4	7	8	15	16	-1
L ₅	0	3	4	7	8	16	17	-1
L ₆	0	4	6	8	11	17	18	-1
L ₇	0	1	2	6	8	12	18	19
L ₈	0	4	5	8	10	19	20	-1
L ₉	0	4	5	8	11	20	21	-1
L ₁₀	1	3	4	8	9	21	22	-1
L ₁₁	0	1	3	4	10	22	23	-1
L ₁₂	0	2	4	7	8	11	12	23

Table II: Block index matrix β_I showing the valid blocks (highlighted) to be processed.

and β_S hold the index locations and the shift values (and hence the connections between the CNs and VNs) corresponding to *only* the valid blocks in \mathbf{H}_b , respectively. Construction of β_I is based on the following definition,

Definition 3. Construction of β_I is as follows.

for $u = \{1, 2, \dots, I\}$
 set $w = 0, j_b = 0$
 for $j_b = \{1, 2, \dots, n_b\}$
 $j_b = j_b + 1$
 if $\mathbf{H}_b(u, j_b) \neq -1$
 $w = w + 1; \beta_I(u, w) = j_b; \beta_S(u, w) = \mathbf{H}_b(u, j_b).$

To observe the benefit of this alternate representation, let us define the following ratio.

Definition 4. Let λ denote the compaction ratio, which is the ratio of the number of columns of β_I (which is the same for β_S) to the number of columns of \mathbf{H}_b . Hence, $\lambda = \frac{J}{n_b}$.

The compaction ratio λ is a measure of the compaction achieved by the alternate representation of H_b . Compared to the conventional approach, scheduling as per the β_I and β_S matrices improves throughput by $\frac{1}{\lambda}$ times. In our case study, $\lambda = \frac{8}{24} = \frac{1}{3}$, thus providing a throughput gain of $\frac{1}{\lambda} = 3$.

Remark 2. In the irregular QC-LDPC code in our case study, all layers comprise of 7 blocks each, except layer L_7 and

L_{12} which have 8. With the aim of minimizing hardware complexity by maintaining a static memory-address generation pattern (does not change from layer-to-layer), our implementation assumes regularity in the code. The decoder processes 8 blocks for each layer of the β_I matrix resulting in some throughput penalty.

E. Layer-Pipelined Decoder Architecture

In Section III-C we saw how dependent layers for a block column cannot be processed in parallel. For instance, in \mathbf{H}_b in Table I, VNs associated with the block column B_1 participate in CN equations associated with all the layers except layer L_{10} , suggesting that there is no scope of parallelization of layer processing at all. This situation is better observed in β_I shown in Table II.

Fact 3. If a block column of β_I has a particular index value appearing in more than one layer, then the layers corresponding to that value are dependent with respect to that block column.

Proof: Follows directly by applying Fact 2 to Definition 3. ■

In other words, $\forall u, u' \in \{1, 2, \dots, I\}, \forall w \in \{1, 2, \dots, J\}$, if, $\beta_I(u, w) = \beta_I(u', w)$ then, the layers L_u and $L_{u'}$ are dependent. It is obvious that, to process all layers in parallel (L_1 to L_{12} in I), the condition,

$$\beta_I(u, w) \neq \beta_I(u', w) \quad (10)$$

must hold for $\forall u, u' \in \{1, 2, \dots, I\}$. We call the set of layers \mathcal{L} satisfying Fact 3 as a *superlayer*. As will be seen later, the formation of superlayers of suitable size is crucial to achieve parallelism in the architecture.

The idea is to rearrange the β_I matrix elements from their original order. If $\beta_I(u, w) = \beta_I(u', w)$, $u < u'$ then *stagger* the execution of $\beta_I(u', w)$ with respect to $\beta_I(u, w)$ by placing $\beta_I(u', w)$ in $\beta'_I(u', w')$ such that, $w < w'$. To understand how layers are pipelined, let us first look at the non-pipelined case.

Without loss of generality, Fig. 2(a) shows the block-level view of the NPU timing diagram without the pipelining of layers. As seen in Section III-A, the GNPU and LNPU operate in tandem and in that order, implying that the LNPU has to wait for the GNPU updates to finish. The layer-level picture is depicted in Fig. 3(a). We call this version as the $1x$ version. This idling of the GNPU and LNPU can be avoided by introducing pipelined processing of blocks given by the following Lemma.

Lemma 1. Within a superlayer, while the LNPU processes messages for the blocks $\beta'(u, w)$, the GNPU can process messages for the blocks $\beta'(u + 1, w)$, $u = \{1, 2, \dots, |\mathcal{L}| - 1\}$ and $w = \{1, 2, \dots, J\}$.

Proof: Follows directly from the layer independence condition in Fact 2. ■

Fig. 2(c) illustrates the block-level view of this 2-layer pipelining scheme. It is important to note that, the splitting of the NPU process into two parts, namely, the GNPU and the LNPU

Layers ↓	Blocks →							
	b ₁	b ₂	b ₃	b ₄	b ₅	b ₆	b ₇	b ₈
L ₁	0	4	8	13	6	10	12	-1
L ₂	9	0	4	8	13	14	2	-1
L ₃	15	9	0	4	8	5	14	-1
L ₄	7	15	16	0	4	8	1	-1
L ₅	17	7	3	16	0	4	8	-1
L ₆	6	17	18	11	-1	0	4	8
L ₇	19	6	0	8	1	2	18	12
L ₈	4	19	5	0	8	20	10	-1
L ₉	21	4	11	5	0	8	20	-1
L ₁₀	1	21	4	3	22	9	8	-1
L ₁₁	0	1	23	4	3	22	10	-1
L ₁₂	8	0	2	23	4	12	7	11

Table III: Rearranged Block Index Matrix β'_I used for our work, showing the valid blocks (highlighted) to be processed.

(that work in tandem) is a necessary condition for Fact 3 (and hence Lemma 1) to hold. However, at the boundary of the superlayer the Lemma 1 does not hold and pipelining has to be restarted for the next layer as seen in the layer-level view shown in Fig. 3(c). We call this version as the $2x$ version. This is the classical pipelining overhead. In the following, we impose certain constraints on the size of the superlayers in **H**.

Definition 5. Without loss of generality, the pipelining efficiency η_p is the number of layers processed per unit time per NPU array.

For the case of pipelining two layers shown in Fig. 3(c),

$$\eta_p^{(2)} = \frac{|\mathcal{L}|}{|\mathcal{L}| + 1} \quad (11)$$

Thus, we impose the following conditions on $|\mathcal{L}|$:

- 1) Since, two layers are processed in the pipeline at any given time, provided that I is even,

$$|\mathcal{L}| \in \mathcal{F} = \{x : x \text{ is an even factor of } I\}.$$

It is important to note that, for any value of $|\mathcal{L}| \in \mathcal{F}$, \mathcal{L} must be a superlayer.

- 2) Given a QC-LDPC code, $|\mathcal{L}|$ is a constant. This is to facilitate a symmetric pipelining architecture which is a scalable solution.
- 3) Choice of $|\mathcal{L}|$ should maximize pipelining efficiency η_p ,

$$l^* = \arg \max_{|\mathcal{L}| \in \mathcal{F}} \eta_p$$

Case Study: Table III shows one such rearrangement of β_I for the QC-LDPC code for our case study in Table II.

Unresolved dependencies are shown in blue in Table III. $I = m_b = 12$, $\mathcal{F} = \{2, 4, 6\}$ and, $l^* = \arg \max_{|\mathcal{L}| \in \mathcal{F}} \eta_p = 6$. The rearranged block index matrix β'_I is shown in Table III and the layer-level view of the pipeline timing diagram for the same is shown in Fig. 3(d).

High-level FPGA-based Decoder Architecture: The high-level decoder architecture is shown in Fig. 4. The ROM holds the LDPC code parameters specified by the β'_I and the β'_s along with other code parameters such as the block length and the maximum number of decoding iterations. The APP memory is initialized with the channel LLR values corresponding to all the VNs as per equation (1). The barrel shifter operates on blocks of VNs (APP values in equation (4)) of size $z \times f$, where f is the fixed-point word length used in the implementation for APP values. It circularly rotates the values to the right by using the shift values from the β'_s matrix in the ROM, effectively implementing the connections between the CNs and VNs. The cyclically shifted APP memory values and the corresponding CN message values for the block in question are fed to the NPU arrays. Here, the GNPU's compute VN messages as per equation (2) and the LNPU's compute CN messages as per equation (3). These messages are then stored back at their respective locations in the RAMs for processing the next block.

IV. CASE STUDY

To evaluate the proposed strategies for achieving high-throughput, we have implemented the scaled-MSA based decoder for the QC-LDPC code in the IEEE 802.11n (2012). For this code, $m_b \times n_b = 12 \times 24$, $z = 27, 54$ and 81 resulting in code lengths of $n = 24 \times z = 648, 1296$ and 1944 bits respectively. Our implementation supports the submatrix size of $z = 81$ and hence is capable of supporting all the block lengths for the rate $R = \frac{1}{2}$ code. At the time of writing this paper, we have successfully implemented the two aforementioned versions.

1) $1x$: The block-level and the layer-level view of the pipelining is illustrated in Fig. 2(b) and 3(b) respectively.

2) $2x$: Pipelining is done in software at the algorithmic description level. The block and layer level views of the pipelined processing are shown in Fig. 2(d) and 3(d) respectively. With an efficiency $\eta_p^{(2)} = 0.86$, the $2x$ version is 1.7 times faster than the $1x$ version.

We represent the input LLRs from the channel and the CTV and VTC messages with 6 signed bits and 4 fractional bits. Fig. 5 shows the bit-error rate (BER) performance for the floating-point and the fixed-point data representation with 8 decoding iterations. As expected, the fixed-point implementation suffers by about 0.5dB compared to the floating point version. The decoder algorithm was described using the *LabVIEW CSDS* software. The *FPGA IP* compiler was then used to generate the VHDL code from the graphical dataflow description. The VHDL code was synthesized, placed and routed using the *Xilinx Vivado* compiler on the *Xilinx Kintex-7* FPGA available on the *NI PXIe-7975R* FPGA board. The decoder core achieves

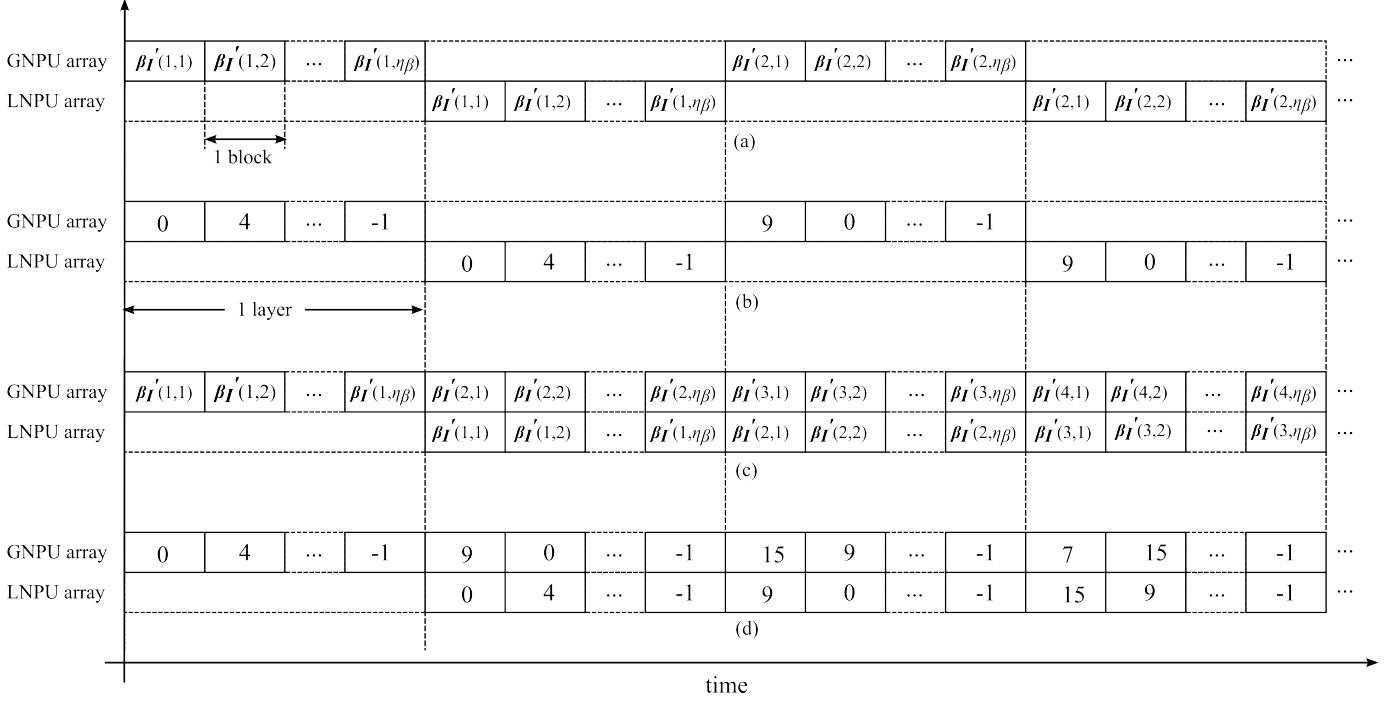


Figure 2: Block-level view of the pipeline timing diagram. (a) General case for a circulant-1 identity submatrix construction based QC-LDPC code (see Section II) without pipelining. (b) Special case of the IEEE 802.11n QC-LDPC code used in this work without pipelining (c) Pipelined processing of two layers for the general QC-LDPC code case in (a). (d) Pipelined processing of two layers for the IEEE802.11n QC-LDPC code case in (b).

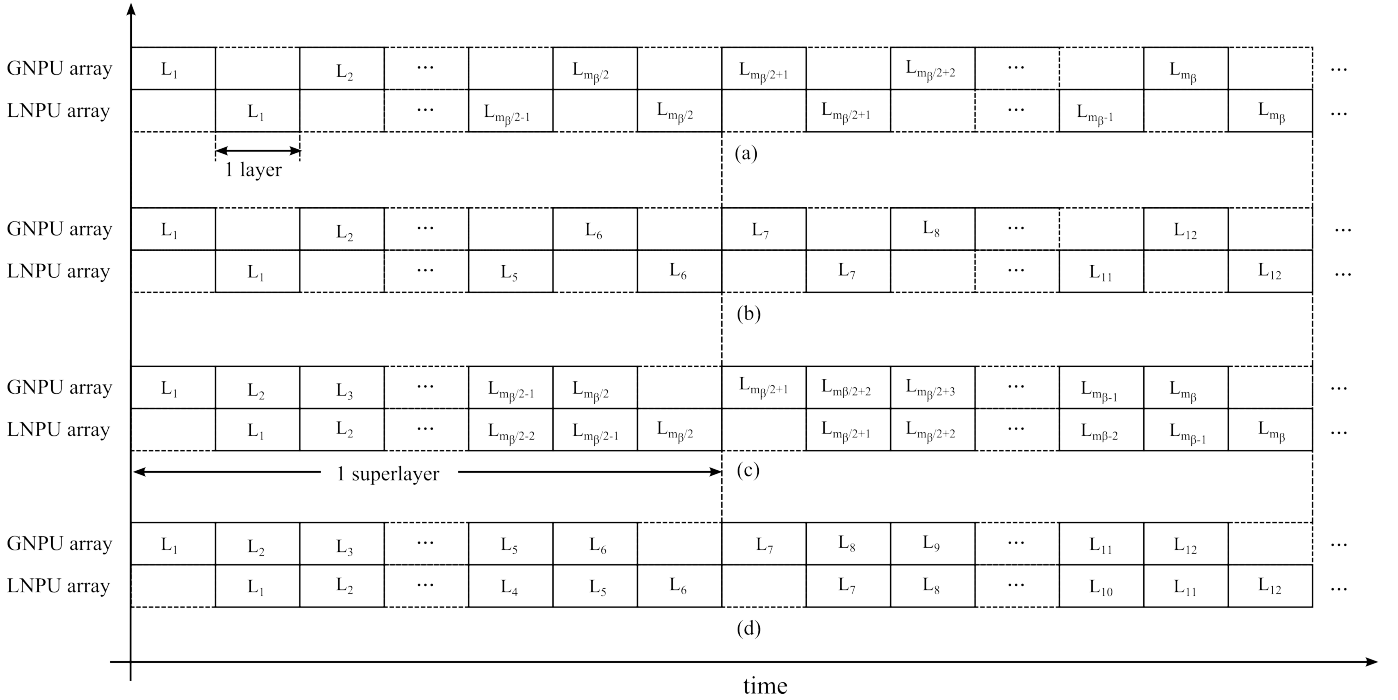


Figure 3: Layer-level view of the pipeline timing diagram. (a) General case for a circulant-1 identity submatrix construction based QC-LDPC code (see Section II) without pipelining. (b) Special case of the IEEE 802.11n QC-LDPC code used in this work without pipelining (c) Pipelined processing of two layers for the general QC-LDPC code case in (a). (d) Pipelined processing of two layers for the IEEE802.11n QC-LDPC code case in (b).

z : submatrix size
 n : codeword length
 N : number of columns in H_p
 d_c : check node (CN) degree
 f : implementation word length

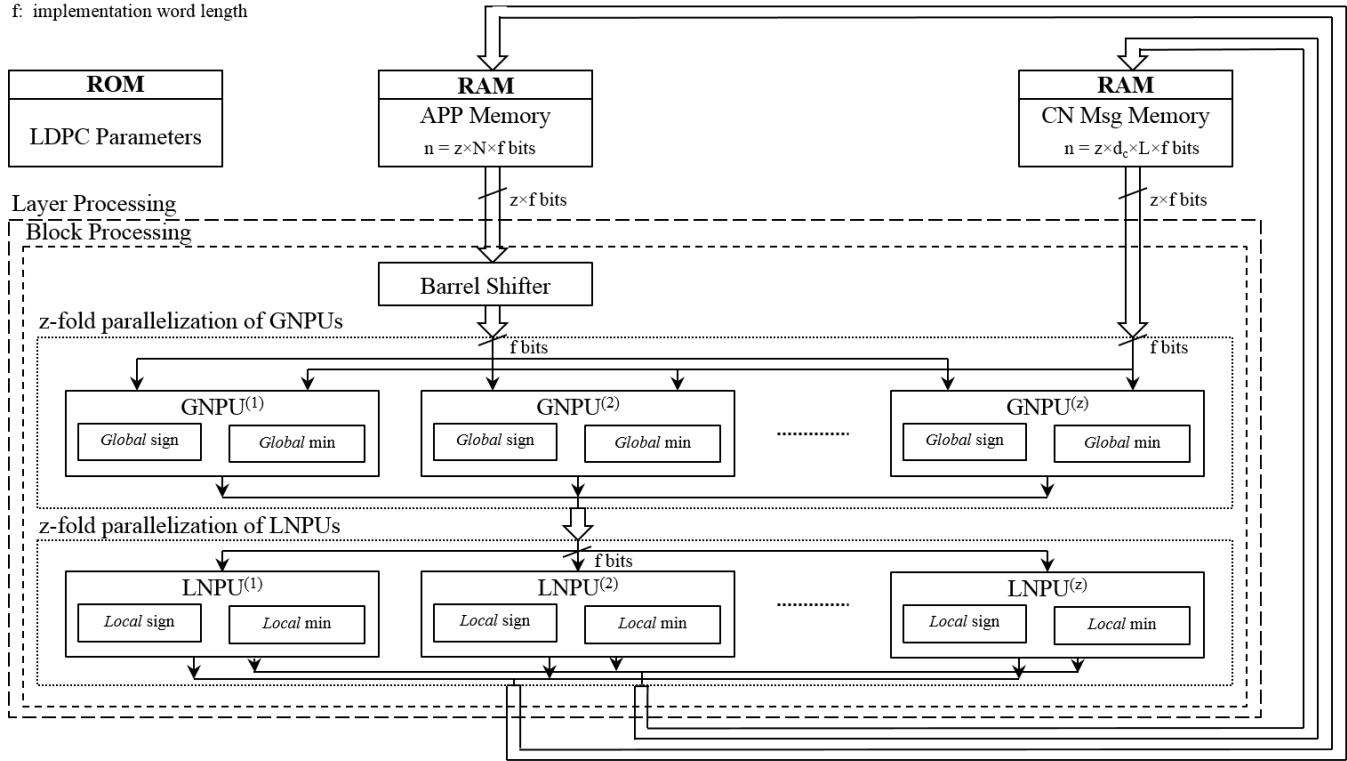


Figure 4: High-level decoder architecture. showing the z -fold parallelization of the NPUs with an emphasis on the splitting of the sign and the minimum computation given in equation (3). Note that, other computations in equations (1)-(4) are not shown for simplicity here. For both the pipelined and the non-pipelined versions, processing schedule for the inner Block Processing loop is as per Fig. 2 and that for the outer Layer Processing loop is as per Fig. 3.

an overall throughput of 608Mb/s at an operating frequency of 200MHz and a latency of $5.7\mu s$. Table IV shows that the resource usage for the $2x$ version (almost twice as fast due to pipelining) is close to that of the $1x$ version. The FPGA IP compiler chooses to use more FF for data storage in the $1x$ version, while it uses more BRAM in $2x$ version. Compared to a contemporary FPGA-based implementation in [14] using high-level algorithmic description compiled to an HDL, our implementation achieves a higher throughput with relatively lesser resource utilization. Authors of [14] have implemented a decoder for a $R = \frac{1}{2}$, $n = 648$, IEEE 802.11n (2012) code that achieves a throughput of 13.4Mb/s at 122MHz, utilizes 2% of slice registers, 3% of slice LUTs and 20.9% of Block RAMs on the *Spartan-6 LX150T* FPGA with a comparable BER performance.

2.06 Gb/s LDPC Decoder [15]: An application of this work has been demonstrated in *IEEE GLOBECOM'14* where the QC-LDPC code for our case study was decoded with a throughput of 2.06 Gb/s. This throughput was achieved by using five decoder cores in parallel on the *Xilinx K7 (410t)* FPGA in the NI USRP-2953R.

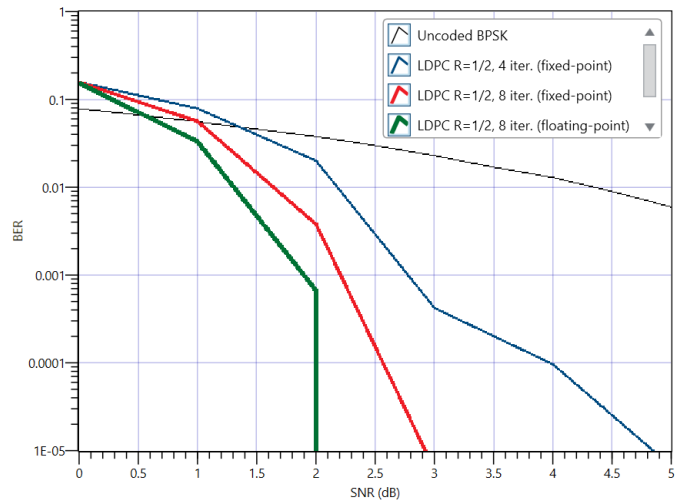


Figure 5: Bit Error Rate (BER) performance comparison between uncoded BPSK (rightmost), rate=1/2 LDPC with 4 iterations using fixed-point data representation (second from right), rate=1/2 LDPC with 8 iterations using fixed-point data representation (third from right), rate=1/2 LDPC with 8 iterations using floating-point data representation (leftmost).

	1x	2x
Device	<i>Kintex-7k410t</i>	<i>Kintex-7k410t</i>
Throughput(Mb/s)	337	608
FF(%)	9.1	5.3
BRAM(%)	4.7	6.4
DSP48(%)	5.2	5.2
LUT(%)	8.7	8.2

Table IV: LDPC Decoder IP FPGA Resource Utilization & Throughput on the Xilinx *Kintex-7* FPGA.

V. CONCLUSION

In this brief we have proposed techniques to achieve high-throughput performance for a MSA based decoder for QC-LDPC codes. We have shown that, with a compact representation of the PCM, significant improvement in throughput can be achieved. A MSA based decoder for the IEEE 802.11n (2012) standard is implemented which achieves a throughput of 608Mb/s (fastest as per our knowledge for an algorithmic compiler) at an operating frequency of 200MHz and a latency of $5.7\mu\text{s}$ on the *Xilinx Kintex-7* FPGA using the *FPGA IP* compiler available in the *National Instruments LabVIEW CSDS* software. The generality of the algorithmic modifications and the methods used to achieve high-throughput results in a scalable decoder architecture which, with little or no modifications can be applied to a family of standard accepted QC-LDPC codes.

ACKNOWLEDGMENT

The authors would like to thank the Department of Electrical & Computer Engineering, Rutgers University for their continual support for this research work and the LabVIEW FPGA R&D and the Advanced Wireless Research team in National Instruments for their valuable feedback and support.

REFERENCES

- [1] "IEEE Standard for Information technology–Telecommunications and information exchange between systems Local and metropolitan area networks–Specific requirements Part 11: Wireless LAN Medium Access Control (MAC) and Physical Layer (PHY) Specifications," *IEEE P802.11-REVmb/D12*, November 2011, pp. 1–2910, March 2012.
- [2] B. Raaf, W. Zirwas, K.-J. Friederichs, E. Tirola, M. Laitila, P. Marsch, and R. Wichman, "Vision for Beyond 4G broadband radio systems," in *Personal Indoor and Mobile Radio Communications (PIMRC), 2011 IEEE 22nd International Symposium on*, Sept 2011, pp. 2369–2373.
- [3] M. Cudak, A. Ghosh, T. Kovarik, R. Ratasuk, T. Thomas, F. Vook, and P. Moorut, "Moving Towards Mmwave-Based Beyond-4G (B-4G) Technology," in *Vehicular Technology Conference (VTC Spring), 2013 IEEE 77th*, June 2013, pp. 1–5.
- [4] R. G. Gallager, "Low-density parity-check codes," *Information Theory, IRE Transactions on*, vol. 8, no. 1, pp. 21–28, 1962.
- [5] D. Costello and S. Lin, *Error control coding*. Pearson, 2004.
- [6] R. Tanner, "A recursive approach to low complexity codes," *Information Theory, IEEE Transactions on*, vol. 27, no. 5, pp. 533–547, Sep 1981.
- [7] F. Kschischang, B. Frey, and H.-A. Loeliger, "Factor graphs and the sum-product algorithm," *Information Theory, IEEE Transactions on*, vol. 47, no. 2, pp. 498–519, Feb 2001.

- [8] E. Sharon, S. Litsyn, and J. Goldberger, "Efficient Serial Message-Passing Schedules for LDPC Decoding," *Information Theory, IEEE Transactions on*, vol. 53, no. 11, pp. 4076–4091, Nov 2007.
- [9] M. Mansour and N. Shanbhag, "High-throughput LDPC decoders," *Very Large Scale Integration (VLSI) Systems, IEEE Transactions on*, vol. 11, no. 6, pp. 976–996, Dec 2003.
- [10] J. Chen and M. Fossorier, "Near optimum universal belief propagation based decoding of ldpc codes and extension to turbo decoding," in *Information Theory, 2001. Proceedings. 2001 IEEE International Symposium on*, 2001, pp. 189–.
- [11] K. Gunnam, G. Choi, M. Yearly, and M. Atiquzzaman, "VLSI Architectures for Layered Decoding for Irregular LDPC Codes of WiMax," in *Communications, 2007. ICC '07. IEEE International Conference on*, June 2007, pp. 4542–4547.
- [12] Y. Sun and J. Cavallaro, "VLSI Architecture for Layered Decoding of QC-LDPC Codes With High Circulant Weight," *Very Large Scale Integration (VLSI) Systems, IEEE Transactions on*, vol. 21, no. 10, pp. 1960–1964, Oct 2013.
- [13] K. Zhang, X. Huang, and Z. Wang, "High-throughput layered decoder implementation for quasi-cyclic LDPC codes," *Selected Areas in Communications, IEEE Journal on*, vol. 27, no. 6, pp. 985–994, August 2009.
- [14] E. Scheiber, G. H. Bruck, and P. Jung, "Implementation of an LDPC decoder for IEEE 802.11n using Vivado TM High-Level Synthesis."
- [15] H. Kee, D. Uliana, A. Arnesen, N. Petersen, T. Ly, A. Aziz, S. Mhaske, and P. Spasojevic, "Demonstration of a 2.06Gb/s LDPC Decoder," in *IEEE Global Communications Conference*, Dec 2014, <https://www.youtube.com/watch?v=o58keq-eP1A>.